ChemComm

COMMUNICATION

View Article Online
View Journal | View Issue

Cite this: *Chem. Commun.*, 2019, 55, 2656

Received 8th January 2019,
Accepted 30th January 2019

DOI: 10.1039/c9cc00166b

rsc.li/chemcomm

Synthesis of photo-excited Chlorin e6 conjugated silica nanoparticles for enhanced anti-bacterial efficiency to overcome methicillin-resistant *Staphylococcus aureus*†

Jia-fu Lin,‡[a] Juan Li,‡[a] Ashna Gopal,[b] Tasnim Munshi,[c] Yi-wen Chu,[a] Jiang-xia Wang,[a] Ting-ting Liu,[a] Bingyang Shi,[d] Xianfeng Chen *[b] and Li Yan *[ae]

Multidrug resistant bacterial infection remains a significant public concern. In this report, photosensitizer Chlorin e6 doped silica was synthesized. This hybrid structure exhibits enhanced photostability and high antibacterial efficiency towards *Staphylococcus aureus* (*S. aureus*) and methicillin-resistant *S. aureus* (MRSA). In summary, this work demonstrates an effective platform to improve the efficiency of antibiotics for better treatment of wound infections.

The use of antibiotics advances modern medicine, and it is an essential tool for almost all medical intervention processes.[1] However, despite the continuous development of antibiotics, bacterial infection remains a significant public concern, particularly over the past few years, since bacteria are generating increasing resistance towards the currently available antibiotics, and the generation of bacterial resistance to antibiotics always surpasses the development process for new ones.[2–7] As a result, this leads to emerging antibiotic-resistant "superbugs", which increase the death toll related to bacterial infection.[8,9] Among these, multi-drug resistant Gram-positive organisms are major vital pathogens that cause serious infections, such as methicillin-resistant *Staphylococcus aureus* (MRSA). MRSA has been ranked to be one of the world's most dangerous bacteria by the World Health Organization (WHO).[10–12]

To tackle the issue of bacterial infection, there has been great effort dedicated to developing new antibiotics. In addition to researching new antibiotics, nanomaterials have been employed as tools to significantly increase drug efficacy. For example, silver, silica, zinc oxide, graphene and polymer nanoparticles have been utilized to inhibit the growth of bacteria.[13–21] These nano-systems have attractive merits for the treatment of bacterial infection, namely their ease of surface functionalization, high antibacterial efficacy and ability to overcome bacterial resistance.[22–25] Among them, mesoporous silica nanoparticles are biodegradable, leading to excellent biocompatibility and biosafety, and the convenience of maintaining the release of bio-active molecules during their degradation.[26–28] All of these advantages make silica nanoparticles a desirable candidate for the delivery of antibiotics. Particularly, Song *et al.* recently reported that silica nanopollens with surface roughness can load an antimicrobial enzyme, lysozyme, and achieve significantly enhanced adhesion to bacteria for long-term bacterial inhibition in comparison to those with a smooth surface.[29] This characteristic further facilitates the application of silica nanoparticles.

Besides using antibiotics for antimicrobial chemotherapy, photodynamic therapy (PDT) has also been applied to fight bacteria.[30–32] In PDT, singlet oxygen is generated in the presence of a photosensitizer and oxygen under light illumination, causing fatal damage to bacteria.[33–36] The application of PDT has been growing rapidly, because it significantly improves antibacterial efficacy and can effectively alleviate drug resistance.[37] However, the poor photostability of photosensitizers and low bacterial affinity hinder their successful applications. Inspired by the success of using surface nanostructures for enhanced antimicrobial/anticancer chemotherapy,[29,38,39] we first report a way to synthesize a silica nanomaterial carrying photosensitizer molecules for a potent photodynamic therapy to treat *Staphylococcus aureus* (*S. aureus*) and MRSA (Scheme 1). This simple technique is expected to enhance the stability of the photosensitizer in the silica matrix, efficiently inhibit bacteria and overcome multi-drug resistance.

Silica nanoparticles are formed using a modified Stöber synthesis solution, followed by treatment at 500 °C for 5 h to remove

[a] *Antibiotics Research and Re-evaluation Key Laboratory of Sichuan Province, Sichuan Industrial Institute of Antibiotics (SIIA), Chengdu University, Chengdu, 610052, Sichuan, P. R. China. E-mail: tony_yan8@hotmail.com, tony.yan@monash.edu*
[b] *School of Engineering, Institute for Bioengineering, The University of Edinburgh, King's Buildings, Mayfield Road, Edinburgh, EH9 3JL, UK. E-mail: xianfeng.chen@oxon.org, Michael.Chen@ed.ac.uk*
[c] *School of Chemistry, University of Lincoln, Brayford Pool, Lincoln, Lincolnshire LN6 7TS, UK*
[d] *Department of Biomedical Sciences, Faculty of Medicine & Health Sciences, Macquarie University, Sydney, NSW, 2109, Australia*
[e] *Monash Institute of Pharmaceutical Sciences, Monash University, Parkville, Victoria 3052, Australia*

† Electronic supplementary information (ESI) available. See DOI: 10.1039/c9cc00166b

‡ Equal contribution.

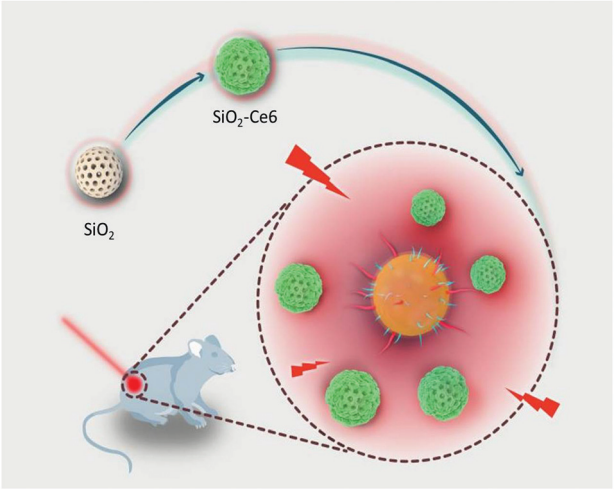

Scheme 1 Schematic illustration of Ce6 doped silica nanoparticle fabrication and photo-inspired disinfection.

the template surfactant during fabrication. Then, (3-aminopropyl)-triethoxysilane (APTES) conjugated Chlorin e6 (Ce6) molecules are incubated with silica nanoparticles, enabling Ce6 loading and creating a rough surface. Their X-ray diffraction (XRD) pattern indicates that these silica nanoparticles are amorphous (MCM-Ce6) (Fig. S1A, ESI†). The Fourier Transform Infrared (FT-IR) spectra of MCM-Ce6 and Ce6 display identical Ce6 peaks, confirming successful conjugation of Ce6 to silica (Fig. S1B, ESI†). The loading capacity of Ce6 is approximately 7.8 wt%, which was measured by absorbance at 400 nm. The morphology of MCM-Ce6 was characterized by transmission electron microscopy (TEM) and scanning electron microscopy (SEM) (Fig. 1A and B). It can be seen that the diameter of these silica nanoparticles is approximately 80–150 nm and these nanoparticles have very rough surfaces.

Next, the optical properties and singlet oxygen generation capacity of MCM-Ce6 were evaluated (Fig. S2 and S3 ESI†). As shown in the UV–vis absorption spectrum, it is clear that Ce6 modified silica nanoparticles exhibit very similar absorption characteristics to free Ce6, further indicating successful conjugation of Ce6 to silica nanoparticles (Fig. S2A, ESI†). Subsequently, the photostability of MCM-Ce6 was tested and compared to that of free Ce6 by exposing the materials to 650 nm light for different time periods (Fig. S2B and S3, ESI†) followed by the absorbance intensity measurement at 400 nm. The results show that after 10 minutes of light irradiation, MCM-Ce6 possesses an absorbance intensity of 70% of the original value; while in sharp contrast, the absorbance of free Ce6 molecules substantially drops to below 30%. This observation demonstrates that the photostability of Ce6 has been significantly improved with covalent conjugation to silica nanoparticles.

The capacity of singlet oxygen generation by the MCM-Ce6 and free Ce6 molecules was also studied using 1,3-diphenylisobenzofuran (DPBF) as a chemical probe. It can be seen that both materials can effectively generate singlet oxygen (Fig. S2C, ESI†). This reveals that the process of doping Ce6 molecules into silica nanoparticles does not induce Ce6 aggregation and

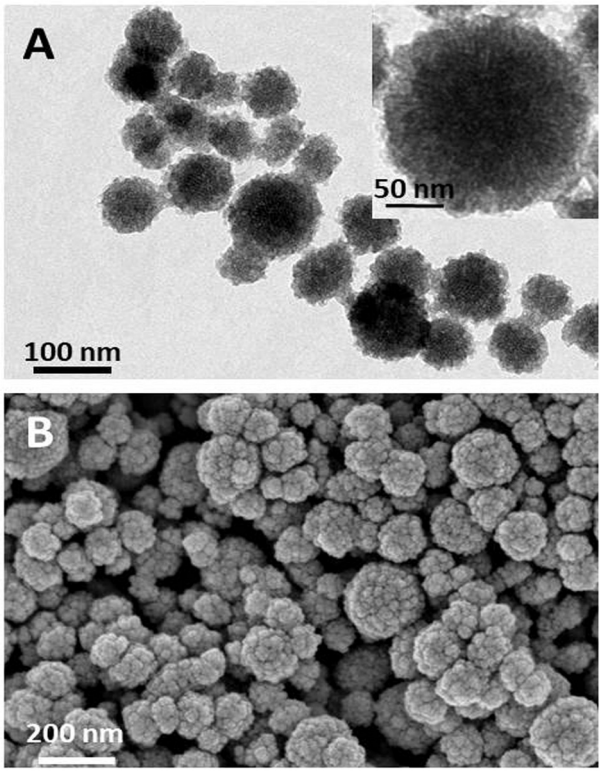

Fig. 1 Characterization of Ce6 doped silica nanoparticles (MCM-Ce6): (A) TEM image and (B) SEM image.

cause decreased capacity of singlet oxygen generation. However, if both materials are exposed to light for 30 minutes before the evaluation of their capacity of singlet oxygen generation, the situation will be different. From Fig. S2D (ESI†), it can be seen that MCM-Ce6 can continuously generate singlet oxygen and cause the absorbance of DPBF to decrease, while free Ce6 molecules produce a very low amount of singlet oxygen. This further confirms the enhanced photostability of Ce6 after being loaded onto silica nanoparticles.

After confirming the improved photostability of MCM-Ce6, its antibacterial performance was next investigated against *S. aureus* and MRSA and the results are presented in Fig. 2 and 3, respectively. *S. aureus* is a common naturally occurring and pathogenic Gram-positive spherical bacterium, while MRSA is a multi-drug resistant bacterium, which causes intractable infections in the clinic. Therefore, effective antibacterial agents to eliminate *S. aureus* and MRSA are highly desirable. In the test, the bacteria were cultured with MCM-Ce6 at different concentrations (200, 66.7, 22.2 and 7.4 μg mL^{-1}) in the presence and absence of light illumination. After treatment, the samples were monitored for turbidity by measuring the optical density (O.D.) at 600 nm. First, the potential risk of killing the bacteria by light irradiation alone was investigated. It is apparent that the light irradiation at our used power intensity did not affect the growth of *S. aureus* and MRSA (control +). At a low concentration of 7.4 μg mL^{-1}, MCM-Ce6 has already exhibited excellent bacterial inhibition for both *S. aureus* and MRSA upon light irradiation (Fig. 2D). In comparison, we also studied the antibacterial

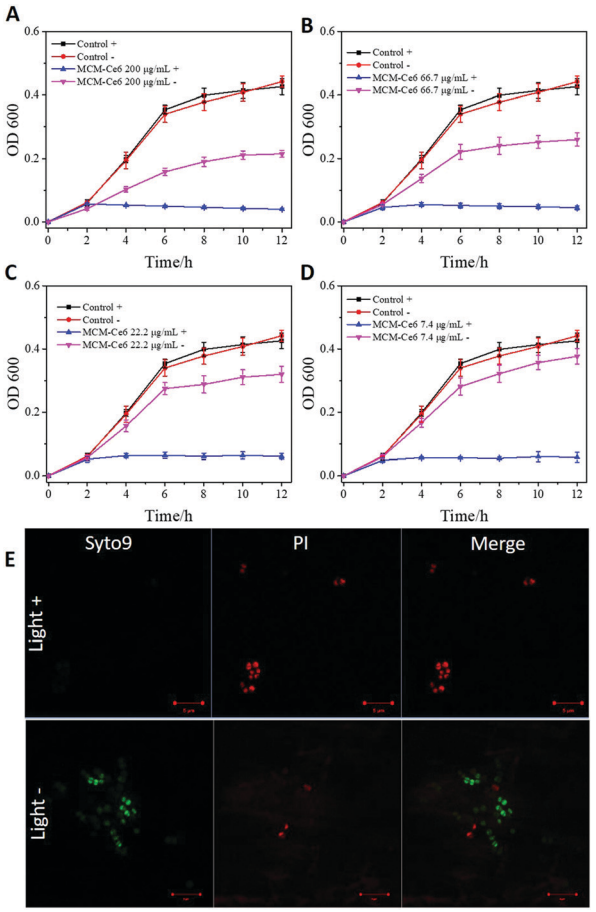

Fig. 2 *S. aureus* inhibition by MCM-Ce6 of different concentrations: (A) 200, (B) 66.7, (C) 22.2 and (D) 7.4 μg mL^{-1}. Control means only LB added. '' +'' indicates with light illumination; ''−'' indicates without light illumination. All data are expressed as mean ± s.d. (indicated by an error bar), based on values obtained from six biological replicates (n = 6). (E) Live/dead analysis of *S. aureus* treated with light (light +) or without light (light −). Scale bars indicate 5 μm.

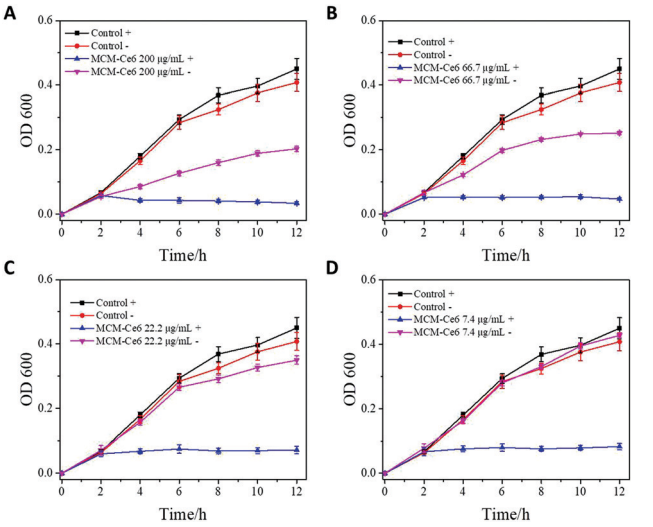

Fig. 3 Methicillin-resistant *S. aureus* inhibition by MCM-Ce6 of different concentrations: (A) 200, (B) 66.7, (C) 22.2 and (D). 7.4 μg mL^{-1}. Control means only LB added. ''+'' indicates with light illumination; ''−'' indicates without light illumination. All data are expressed as mean ± s.d. (indicated by an error bar), based on values obtained from six biological replicates (n = 6).

performance of MCM-Ce6 without light irradiation and the results show dramatically reduced bacterial inhibition efficacy (Fig. 2A–D). This observation clearly demonstrates the contribution of light excitation. To further evaluate the antibacterial performance, live/dead analysis of *S. aureus* was performed (Fig. 2E). Consistent with O.D. measurements, large amounts of killed bacteria were found in the light-treated group. Moreover, the plate count method was carried out after the O.D. measurement. Similar bacterial inhibition profiles were also observed (Fig. S4 and S5, ESI†). In addition, the antibacterial performance of MCM-Ce6 was compared with that of traditional Ce6 conjugated silica nanoparticles. The traditional Ce6 conjugated silica nanoparticles were fabricated by conjugating Ce6 molecules with amine modified silica. It was found that MCM-Ce6 exhibited an obviously improved *S. aureus* inhibition performance compared to traditional Ce6 conjugated silica nanoparticles, particularly after a short exposure period (Fig. S6, ESI†). Therefore, it is very important to conjugate APTES and Ce-6 molecules first and then attach them to silica nanoparticles for enhanced antibacterial performance.

After demonstrating the high efficacy of MCM-Ce6 in antibacterial inhibition *in vitro*, we moved the application to *in vivo* wound healing, utilizing Balb/c mice as a model. A wound was introduced on their back followed by infection with *S. aureus* (Fig. 4). Then the mice were randomly divided into three groups. Two groups of mice were treated with either free Ce6 molecules or MCM-Ce6. The untreated mice were used as a control group. During the treatment, a clear difference in the wound morphology was observed among the groups and the representative images are shown in Fig. 4A. Obviously, scabs were quickly formed in the group of mice treated with MCM-Ce6 under light irradiation. In contrast, it was difficult to even form a scab in the group of mice treated with free Ce6 molecules, indicating poor efficiency in the *in vivo* wound treatment. During the whole treatment period, the mice did not show any obvious body weight change in all experimental groups (Fig. 4B). Fig. 4C shows the H&E staining of the wounded skin harvested from the mice treated with MCM-Ce6, which indicates a well-organised skin structure and good wound-healing effect. In addition, H&E staining of the major organs of the mice treated with MCM-Ce6 under light illumination was also conducted (Fig. S7, ESI†), from which no obvious abnormality was found, indicating excellent compatibility of Ce6 doped silica nanoparticles.

In summary, our study illustrates a strategy to synthesize photosensitizer loaded silica nanoparticles for significantly enhanced photodynamic therapy to effectively inhibit *S. aureus* and MRSA. This drug delivery system improves the photostability of Ce6 molecules and correspondingly maintains the singlet oxygen generation capacity under light illumination. When tested *in vivo*, the drug delivery system dramatically enhances wound healing efficiency in comparison with fee Ce6 molecules.

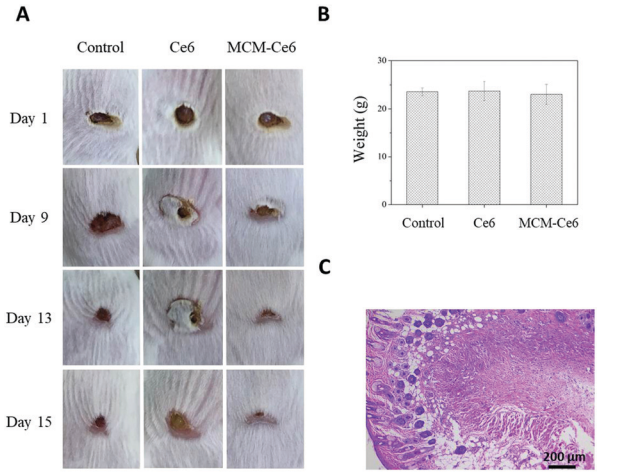

Fig. 4 *In vivo S. aureus* infected wound healing evaluation of Ce6 doped silica (MCM-Ce6). (A) Digital images of wounds infected by *S. aureus*. (B) Body weight of mice treated in different groups. All data are expressed as mean ± s.d. (indicated by an error bar). (C) Hematoxylin and eosin stain of *S. aureus* infected skin tissue sections treated with Ce6 doped silica under light irradiation.

Also importantly, these Ce6 doped silica nanoparticles have excellent biocompatibility. This work is the first report on the use of the nanomaterials' rough surface for increased performance in antibacterial photodynamic therapy and demonstrates an effective platform to improve the efficiency of antibiotics.

The authors acknowledge the support provided by the National Natural Science Foundation of China (No. 81803480), the Chengdu University (No. 2081916010 and ARRLKF16-05), Sichuan Science and Technology Program (No. 2018HH0007), School of Engineering of The University of Edinburgh, and the Royal Society Research Grant Scheme RG150564.

Conflicts of interest

There are no conflicts to declare.

Notes and references

1 J. M. Munita, A. S. Bayer and C. A. Arias, *Clin. Infect. Dis.*, 2015, **61**, S48–S57.
2 D. Mao, F. Hu, Kenry, S. Ji, W. Wu, D. Ding, D. Kong and B. Liu, *Adv. Mater.*, 2018, **30**, 1706831.
3 C. Mao, Y. Xiang, X. Liu, Z. Cui, X. Yang, K. W. K. Yeung, H. Pan, X. Wang, P. K. Chu and S. Wu, *ACS Nano*, 2017, **11**, 9010–9021.
4 C. M. Courtney, S. M. Goodman, J. A. McDaniel, N. E. Madinger, A. Chatterjee and P. Nagpal, *Nat. Mater.*, 2016, **15**, 529–534.
5 X. Yang, J. Yang, L. Wang, B. Ran, Y. Jia, L. Zhang, G. Yang, H. Shao and X. Jiang, *ACS Nano*, 2017, **11**, 5737–5745.
6 L. Liu, K. Xu, H. Wang, P. K. Tan, W. Fan, S. S. Venkatraman, L. Li and Y. Y. Yang, *Nat. Nanotechnol.*, 2009, **4**, 457–463.
7 H. Alhmoud, A. Cifuentes-Rius, B. Delalat, D. G. Lancaster and N. H. Voelcker, *ACS Appl. Mater. Interfaces*, 2017, **9**, 33707–33716.
8 L. Han and S. Che, *Adv. Funct. Mater.*, 2018, **28**, 1705708.
9 X. Fan, F. Yang, C. Nie, Y. Yang, H. Ji, C. He, C. Cheng and C. Zhao, *ACS Appl. Mater. Interfaces*, 2018, **10**, 296–307.
10 Y. Xie, Y. Liu, J. Yang, Y. Liu, F. Hu, K. Zhu and X. Jiang, *Angew. Chem., Int. Ed.*, 2018, **57**, 3958–3962.
11 J. Wang, J. Li, S. Qian, G. Guo, Q. Wang, J. Tang, H. Shen, X. Liu, X. Zhang and P. K. Chu, *ACS Appl. Mater. Interfaces*, 2016, **8**, 11162–11178.
12 D. Hu, H. Li, B. Wang, Z. Ye, W. Lei, F. Jia, Q. Jin, K. F. Ren and J. Ji, *ACS Nano*, 2017, **11**, 9330–9339.
13 C. Cheng, A. He, C. Nie, Y. Xia, C. He, L. Ma and C. Zhao, *J. Mater. Chem. B*, 2015, **3**, 4170–4180.
14 M. He, Q. Wang, J. Zhang, W. Zhao and C. Zhao, *ACS Appl. Mater. Interfaces*, 2017, **9**, 44782–44791.
15 G. Rajeev, B. Prieto Simon, L. F. Marsal and N. H. Voelcker, *Adv. Healthcare Mater.*, 2018, **7**, 1700904.
16 Z. Xu, X. Wang, X. Liu, Z. Cui, X. Yang, K. W. K. Yeung, J. C. Chung, P. K. Chu and S. Wu, *ACS Appl. Mater. Interfaces*, 2017, **9**, 39657–39671.
17 C. Li, X. Wang, F. Chen, C. Zhang, X. Zhi, K. Wang and D. Cui, *Biomaterials*, 2015, **34**, 3882–3890.
18 D. G. Yu, J. Zhou, N. P. Chatterton, Y. Li, J. Huang and X. Wang, *Int. J. Nanomed.*, 2012, **7**, 5725–5732.
19 C. D. Tran, J. Makuvaza, E. Munson and B. Bennett, *ACS Appl. Mater. Interfaces*, 2017, **9**, 42503–42515.
20 J. Gao, H. Gu and B. Xu, *Acc. Chem. Res.*, 2009, **42**, 1097–1107.
21 W. Zhang, S. Shi, Y. Wang, S. Yu, W. Zhu, X. Zhang, D. Zhang, B. Yang, X. Wang and J. Wang, *Nanoscale*, 2016, **8**, 11642.
22 W. Hong, Y. Zhao, Y. Guo, C. Huang, P. Qiu, J. Zhu, C. Chu, H. Shi and M. Liu, *ACS Appl. Mater. Interfaces*, 2018, **10**, 10688–10705.
23 G. Hazell, L. E. Fisher, W. A. Murray, A. H. Nobbs and B. Su, *J. Colloid Interface Sci.*, 2018, **528**, 389–399.
24 M. Li, Q. Liu, Z. Jia, X. Xu, Y. Shi, Y. Cheng and Y. Zheng, *J. Mater. Chem. B*, 2015, **3**, 8796–8805.
25 X. Chen, X. Huang, C. Zheng, Y. Liu, T. Xu and J. Liu, *J. Mater. Chem. B*, 2015, **3**, 7020–7029.
26 D. Cassano, M. Summa, S. Pocoví-Martínez, A. K. Mapanao, T. Catelani, R. Bertorelli and V. Voliani, *Part. Part. Syst. Charact.*, 2018, 1800464.
27 C. Avigo, D. Cassano, C. Kusmic, V. Voliani and L. Menichetti, *J. Phys. Chem. C*, 2017, **121**, 6955–6961.
28 D. Ling, L. Gao, J. Wang, M. Shokouhimehr, J. Liu, Y. Yu, M. J. Hackett, P. K. So, B. Zheng, Z. Yao, J. Xia and T. Hyeon, *Chem. – Eur. J.*, 2014, **20**, 7916–7921.
29 H. Song, Y. Ahmad Nor, M. Yu, Y. Yang, J. Zhang, H. Zhang, C. Xu, N. Mitter and C. Yu, *J. Am. Chem. Soc.*, 2016, **138**, 6455–6462.
30 M. F. Wu, M. Deichelbohrer, T. Tschernig, M. W. Laschke, N. Szentmáry, D. Hüttenberger, H. J. Foth, B. Seitz and M. Bischoff, *Sci. Rep.*, 2017, 44537.
31 Z. Zhao, R. Yan, J. Wang, H. Wu, Y. Wang, A. Chen, S. Shao and Y. Q. Li, *J. Mater. Chem. B*, 2017, **5**, 3572–3579.
32 Q. Cai, Y. Fei, H. W. An, X. X. Zhao, Y. Ma, Y. Cong, L. Hu, L. L. Li and H. Wang, *ACS Appl. Mater. Interfaces*, 2018, **10**, 9197–9202.
33 C. Mao, Y. Xiang, X. Liu, Z. Cui, X. Yang, Z. Li, S. Zhu, Y. Zheng, K. W. K. Yeung and S. Wu, *ACS Nano*, 2018, **12**, 1747–1759.
34 H. Zhu, J. Li, X. Qi, P. Chen and K. Pu, *Nano Lett.*, 2018, **18**, 586–594.
35 B. S. Hass and R. B. Webb, *Mutat. Res., Fundam. Mol. Mech. Mutagen.*, 1979, **60**, 1.
36 L. Yan, Z. Wang, X. Chen, X. J. Gou, Z. Zhang, X. Zhu, M. Lan, W. Chen, G. Zhu and W. Zhang, *Chem. Commun.*, 2017, **53**, 2339–2342.
37 Q. Xiao, J. Wu, X. Pang, Y. Jiang, P. Wang, A. W. Leung, L. Gao, S. Jiang and C. Xu, *Curr. Med. Chem.*, 2018, **25**, 839–860.
38 R. Xu, L. Huang, W. Wei, X. Chen, X. Zhang and X. Zhang, *Biomaterials*, 2016, **93**, 38–47.
39 Y. Niu, M. Yu, S. B. Hartono, J. Yang, H. Xu, H. Zhang, J. Zhang, J. Zou, A. Dexter, W. Gu and C. Yu, *Adv. Mater.*, 2013, **25**, 6233–6237.